Accepted for Publication, Journal of the American Ceramic Society, 02/12/2025
http://doi.org/10.1111/jace.20482

The origin of charged domains on the surface of ferroelastic $BiVO_4$ co-doped with Na and Mo

Ajay S. Pisat, Jackson C. Adler, Paul A. Salvador, Gregory S. Rohrer*

Department of Materials Science and Engineering, Carnegie Mellon University, Pittsburgh, Pennsylvania 15213, USA

* corresponding author email: gr20@andrew.cmu.edu

Abstract

Ferroelastic $BiVO_4$ has charged surface domains, even though its crystal structure is non-polar. These charged domains can be detected by piezo-force microscopy and lead to spatially selective photochemical reactions. The photochemical reactivity of $(Bi_{0.96}Na_{0.04})(V_{0.92}Mo_{0.08})O_4$ is studied above and below the ferroelastic transition temperature to better understand the origin of charged ferroelastic domains. The results demonstrate that spatially selective reactivity occurs above the ferroelastic transition temperature, similar to what is observed below the transition temperature. Furthermore, when the sample is cooled after brief excursions above the transition temperature, the domains reform with a microstructure that is indistinguishable from what is observed before the transition. The results are consistent with the idea that inhomogeneous distributions of charged point defects, created by stress in the ferroelastic domains, lead to charged domains that promote spatially selective photochemical reactions. If these inhomogeneous defect distributions are not homogenized above the transition temperature, they can template the re-creation of the original domain microstructure after the transformation back to the ferroelastic phase.

Keywords: photochemistry, ferroelastic, domains, point defects, $BiVO_4$

1. Introduction

$BiVO_4$ is a promising photoanode material for water splitting that is made of inexpensive elements, absorbs visible light (with a band gap of around 2.4 eV), and has an optimal valence band position for water oxidation.[1,2] Bulk[3] and surface[4] recombination of photogenerated charge carriers have been identified as mechanisms that limit its water splitting efficiency. However, $BiVO_4$ also has two different charge separation mechanisms that might be exploited to reduce recombination and improve efficiency. The first is that different surface orientations are relatively more photocathodic and photoanodic.[5-7] For example, the (110) is the more photoanodic orientation and the (010) is the more photocathodic orientation. The second charge separation mechanism in $BiVO_4$ is related to its ferroelastic domains.[8,9] $BiVO_4$ transforms from a tetragonal ($I4_1/a$, a = 5.147 Å, c = 11.7216 Å) to a monoclinic (I2/b, a = 5.1935 Å, b = 5.0898 Å, c = 11.6972 Å, γ = 89.613°) structure while cooling to room temperature and, to minimize the ferroelastic transformation strain, a domain microstructure is formed.[10,11] Neighboring domains are separated by straight walls, across which the crystal is rotated about the c-axis by about 90°.[12,13] The domains are piezo-responsive[8] and alternating domains favor oxidation or reduction.[9]

The separation of photogenerated charge carriers by ferroelastic domains has also been observed in two other centrosymmetric ferroelastics, WO_3[14] and $CaTiO_3$.[15] The observations imply that some domain surfaces are relatively positively (negatively) charged and promote the photocathodic (photoanodic) reaction. However, the origin of this positive and negative charge is not obvious. The structures of $BiVO_4$,[11] WO_3,[16] and $CaTiO_3$[17] are all centrosymetric and, therefore, nonpolar. One of the proposed origins of the surface charge in non-polar materials is the segregation of charged defects to relax strain in the transformed

microstructure.[18,19] A plausible mechanism is that the vacancy formation energy is reduced in domains subjected to tensile stress compared to domains in a compressive stress state. This would create a gradient in the vacancy concentration between domains and, if the vacancies are charged, different charges in adjacent domains. The second proposed explanation is the flexoelectric effect, in which inhomogeneous strain at the free surface breaks the symmetry and creates a locally polar structure.[20] Because the sign of the strain is different in domains with tensile and compressive strains, neighboring domains (with opposite stresses) would have opposite charges.

The two mechanisms described above, charging related to the flexoelectric effect or to defect segregation, are both driven by internal stresses associated with the ferroelastic domains. Because the presence of internal stresses in these transformed microstructures is certain, and these stresses are likely amplified by thermal stresses in the polycrystalline microstructure, it is difficult to absolutely establish the origin of the charged domains. However, there is one notable difference. If the charge is related only to the flexoelectric effect, then it should disappear when $BiVO_4$ is heated to a temperature where the structure is no longer ferroelastic. More importantly, it should disappear almost instantly, because the charge is related to atomic displacements within the elastic limit that should relax very quickly. On the other hand, if point defect segregation is responsible for the charge, then the charged areas of the surface will temporarily remain charged even after the transformation to a non-ferroelastic structure. Atomic diffusion will be required to homogenize the surface charge, and this cannot happen instantaneously.

The purpose of this paper is to determine whether or not the surface charges on the domains of $BiVO_4$ dissipate instantaneously at a temperature where it is no longer

ferroelastic and the domains disappear. As a measure of the surface charge, the photocathodic reduction of Ag^{+} and photoanodic oxidation of Mn^{++} or Pb^{++} from aqueous solutions are used. If the surface charge associated with the domains dissipates immediately, then the photochemical reaction products will be produced uniformly on the surface. If the surface charge remains after the domains have disappeared, then the reduced and oxidized products will be distributed in a pattern similar to the preexisting domains. To make it possible to conduct these experiments in aqueous solutions, the ferroelastic transition temperature was reduced from 255 °C to 70 °C by forming a $(Bi_{1-0.5x}Na_{0.5x}V_{1-x}Mo_x)O_4$ solid solution with x = 0.08. The patterns of photochemical reaction products formed at 85 °C demonstrate that domain related charges persist after the domains have disappeared, supporting the idea that charge arises from charged point defect segregation.

2. Experimental Methods

The Na, Mo co-doped $BiVO_4$ ceramics were synthesized using a solid-state reaction of Bi_2O_3 (99.999% pure – Strem Chemicals) and V_2O_5 (99.2 % pure – Johnson Matthey) with appropriate amounts of Na_2CO_3 (99.95 % pure – Alfa Aesar), and MoO_3 (99.95 % pure – Alfa Aesar) followed by sintering. The powders were mixed in a stoichiometric ratio, wet-ground (in ethanol) using a mortar and pestle, and heated in an alumina crucible at 600 °C for 3 h in air. After the grinding and heating cycle was repeated two more times, pellets were formed by adding a small amount of aqueous PVA and pressing the powder in a ½ inch diameter die with a hydraulic press. The samples were then heated at 10 °C/min to 600 °C, held for 2 h, heated at the same rate to 800 °C, held for 20 h, and then cooled at 5 °C/min. The samples were then hand polished with minimal downward pressure using 1200 grit size SiC, followed

sequentially by 3 μm, 1 μm, and 0.05 μm diamond, and finished with 0.02 μm colloidal silica. Finally, the ceramics were annealed at 400 °C for 3 h to heal polishing damage and cooled inertially. The samples remained at room temperature for at least several days before the experiments.

Crystals of $BiVO_4$ were synthesized by a hydrothermal process using parameters similar to those reported by Li et al.[6]. To begin, 36 mmol of NH_4VO_3 and $Bi(NO_3)_3 \bullet 5H_2O$ were mixed in 300 ml of 2 M nitric acid solution. The solution pH was adjusted to 2 by adding ammonia and was then aged for 2 h. The precipitate was transferred to a 100 ml Teflon lined autoclave and filled 50 % of the volume. The autoclave was heated at 3 °C/s to 200 °C, held for 20 h, and the cooled at 5 °C/min. The product was filtered and washed with deionized water.

All room temperature photodeposition measurements were carried out by immersing the samples in a 0.015 M aqueous $AgNO_3$ solution and illuminating for 8.5 to 10 min with a Newport Oriel research arc lamp operated at 150 W. Ceramic samples were fixed to a glass slide using double stick tape and the hydrothermally grown crystals were fixed to carbon tape on an SEM sample stub. Before the samples were illuminated, a viton O-ring was placed on the ceramic surface or the SEM stub, filled with the $AgNO_3$ solution, and closed at the top with a quartz cover slip. After reaction, the samples were immersed in deionized water five times to remove the $AgNO_3$ solution before being dried using compressed air.

For the photodeposition reactions at elevated temperatures, it was necessary to completely degas the apparatus and solution before the experiment to avoid the formation of bubbles at elevated temperature and to minimize the reaction time and effects of evaporation. The sample, O-ring, cover slip, and water used for the solution were placed in a vessel and evacuated. After the pressure reached a constant minimum, the components

were removed and dried and 0.14 g of $Mn(NO_3)_2 \bullet 4H_2O$ (or 0.561 g of $Pb(CH_3COO)_2$ for the Pb marker reaction) was dissolved in 5 ml of the degassed water. The sample, O-ring, solution, and cover slip were assembled as before, but placed on a heater until the solution temperature was measured to be 85 °C (about 4 min). The samples were then exposed to UV light from the arc lamp operated at 300 W for 60 to 75 s. Immediately afterward, the sample was immersed in room temperature de-ionized water, followed by rinsing and drying. Control experiments without illumination were used to verify that heating to 85 °C for 5 min does not cause the spontaneous deposition of the metal salts.

Samples were imaged using an FEI Quanta 200 or Quanta 600 SEM and by atomic force microscopy (AFM) using NT-MDT SOLVER NEXT or NTEGRA AFMs. The AFM images were made using diamond-coated tips from Budget sensors (Tap300DLC) and the data was analyzed using Gwyddion.[21] The Quanta 600 SEM was used for the hot-stage experiment. Images with back scattered electron (BSE) contrast were recorded at intervals of 10 °C from 40 °C to 80 °C using a hook detector. At each temperature, the samples were equilibrated for 5 min before recording the image.

Elevated temperature diffraction was carried out using an improvised hot stage on an X'Pert Pro MPD x-ray diffractometer. The sample was supported on a heater to increase the temperature to 85 °C. Because of the improvised nature of the set-up, it was not possible to situate the sample exactly in the calibrated diffraction plane of the instrument and, as a result, the patterns were shifted by 1° (1.2°) at room temperature (85 °C) so that the peaks matched the positions recorded using the diffractometer in the standard configuration. Note that the signature of the monoclinic (m) to tetragonal (t) phase transition is the coalescence of the $(200)_m$ and $(020)_m$ peaks at room temperature to a single $(200)_t$ peak at elevated

temperature. A small angular shift of the diffraction peaks will not prevent the observation of this change to the diffraction pattern. For this experiment, the X-ray source was operated at 40 kV and 30 mA. To capture the $(200)_m$ and $(020)_m$ peaks, the diffraction pattern was measured in the 2θ range from 33° to 34.45° using a step size of 0.006565°. Diffraction patterns were also collected in 2θ range from 25° to 80° using a step size of 0.026248°.

3. Results

Zhou et al.[22] reported that $(Bi_{1-0.5x}Na_{0.5x})(V_{1-x}Mo_x)O_4$ solid solutions with x = 0.08 have the monoclinic structure at room temperature; the diffraction pattern (See Fig. S1) confirmed our samples with this composition have the same structure. A BSE contrast image of a sample with this composition, shown in Fig. 1, exhibits striped contrast characteristic of the ferroelastic domain structure found in monoclinic samples.[8,9] According to Zhou et al.[22], this material should transform to the tetragonal structure at about 70 °C. Two experiments were carried out to confirm the transition in our samples. In the first experiment, the sample was imaged in the SEM while heating it from room temperature to 70 °C and back to room temperature. The results are shown in Fig. 2, which show domain contrast from electron channeling. A number of parallel domains are clearly observed in the central grain (three of them are labeled 'D' in Fig. 2a). Several residual polishing scratches with similar contrast can also be identified and three are labeled with an 'S' in Fig. 2a for clarity. The horizontal lines on the images are imaging artifacts related to sample charging. While contrast related to the domains is clear in Figs. 2(a) and (b) at 40 °C and 55 °C, respectively, the domain related contrast disappears at 70 °C. When the sample is cooled back to 40 °C, the domain

contrast reappears. The domain pattern after the transformation in Fig. 2d is almost identical to the original pattern.

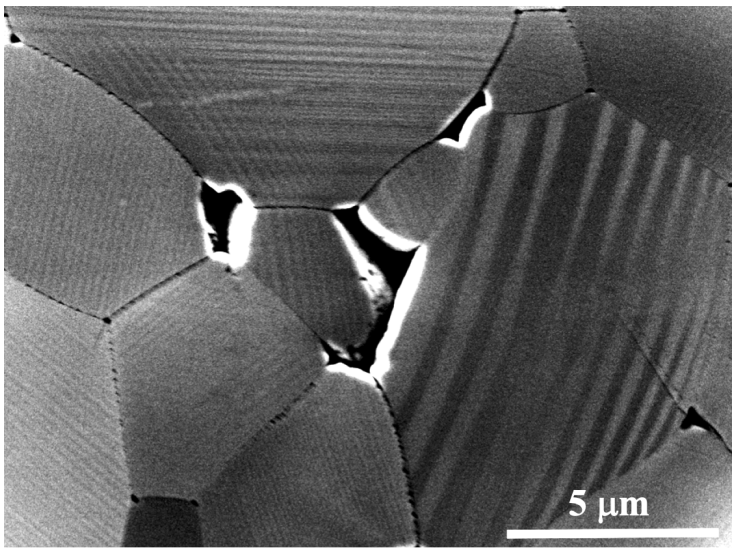

Figure 1. Backscatter electron contrast (BSE) image of the Na, Mo co-doped sample, $(Bi_{1-0.5x}Na_{0.5x})(V_{1-x}Mo_x)O_4$, x = 0.08.

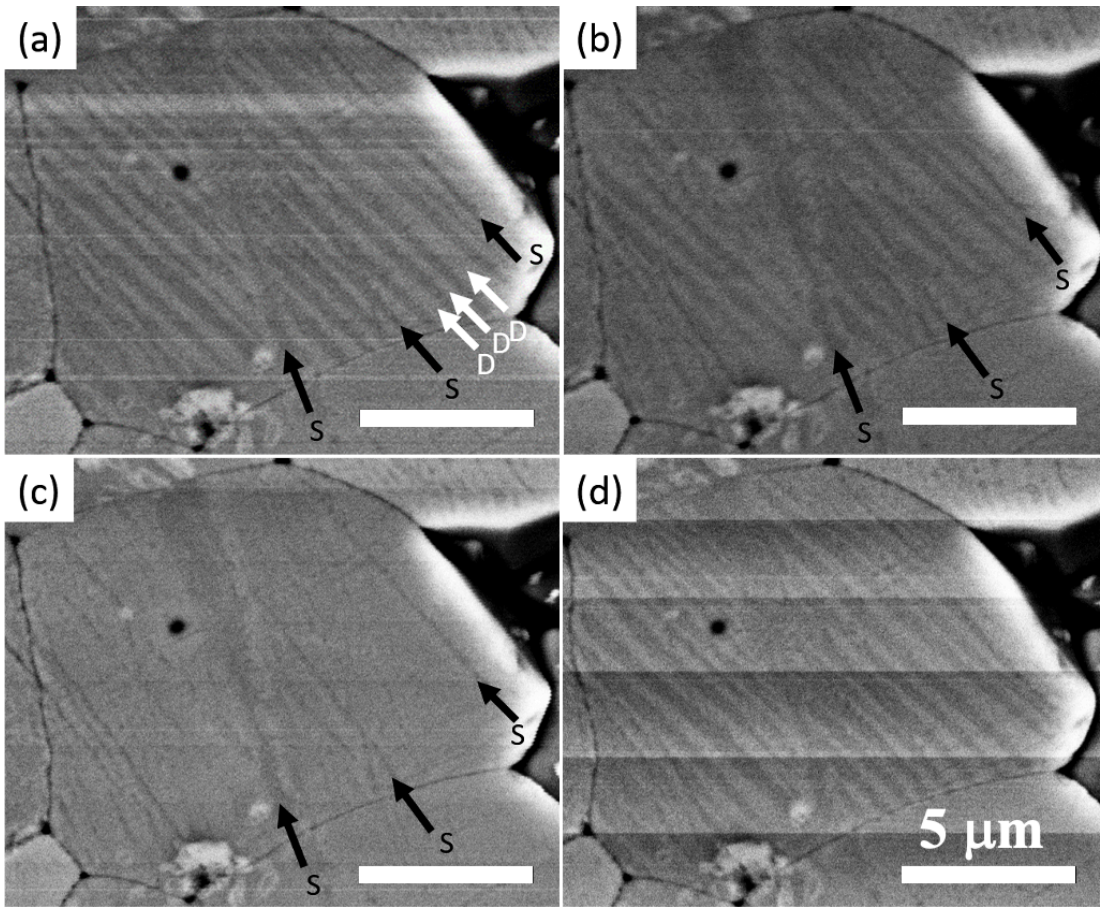

Figure 2. Hot-stage SEM images of a grain in x = 0.08 sample of $(Bi_{1-0.5x}Na_{0.5x}V_{1-x}Mo_x)O_4$ at different temperatures. (a) 40 °C (b) 55 °C (c) 70 °C (d) after cooling back to 40 °C. S denotes scratches and D denotes domains in the images.

While the images in Fig. 2 provide evidence that at least one grain transformed to the tetragonal structure, it is also important to get statistical information, and this was accomplished with X-ray diffraction. Figure 3 shows the part of the XRD diffraction pattern of the co-doped sample at two different temperatures in the range where the (200) and (020) peaks are found ($34.4° < 2\theta < 35.4°$), along with the simulated patterns for monoclinic and tetragonal forms of the sample with the same composition. Here, the splitting of the (200) peak in the tetragonal phase to the (200) and (020) peaks in the monoclinic phase is the signature of the phase transformation.[22] At room temperature (green), the structure is

monoclinic, with two clearly distinct peaks at 34.7° (200) and 35.1° (020). When the sample was held at 85 °C, only a single diffraction peak is observed, at an angle intermediate between the peaks in the monoclinic structure, which indicates that the sample has transformed to the tetragonal structure. Diffraction patterns simulated by Crystal Diffract[23] for the monoclinic and tetragonal structures with the same composition, using the lattice parameters reported by Zhou et al.[22] are consistent with the observed patterns. The diffraction results indicated that the sample has transformed to the tetragonal phase at 85 °C, consistent with the previous work.[22]

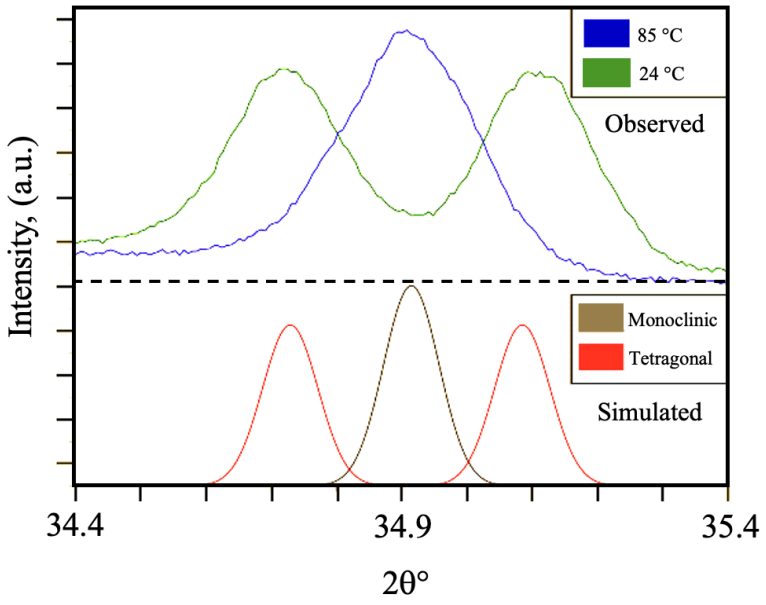

Figure 3. (a) XRD patterns of the x = 0.08 sample of $(Bi_{1-0.5x}Na_{0.5x})(V_{1-x}Mo_x)O_4$ on the hot plate at room temperature (in green) and at 85 °C. (b) Simulated XRD patterns of x = 0.08 co-doped monoclinic (in black) and tetragonal (in pink) $(Bi_{1-0.5x}Na_{0.5x})(V_{1-x}Mo_x)O_4$. The lattice parameters were obtained from[22].

Topographic AFM images of the surface of a sample after the photoanodic deposition of MnO_x are shown in Fig. 4 for the reaction carried out at (a) room temperature and (b) 85 °C. Although MnO_x deposits formed everywhere on the surface, there are more and larger

deposits arranged in a striped pattern. This pattern is found in both images and the stripes are orientated in the same direction. The striped pattern is consistent with the domain structure illustrated in Figs. 1 and 2. The observation that the stripes formed at 85 °C, a temperature where the XRD data and the hot-stage microscopy data tell us that the sample is tetragonal and does not have ferroelastic domains, indicates that there are still surface charges at 85 °C, and they have the same pattern as the original domains (prior to heating to 85 °C).

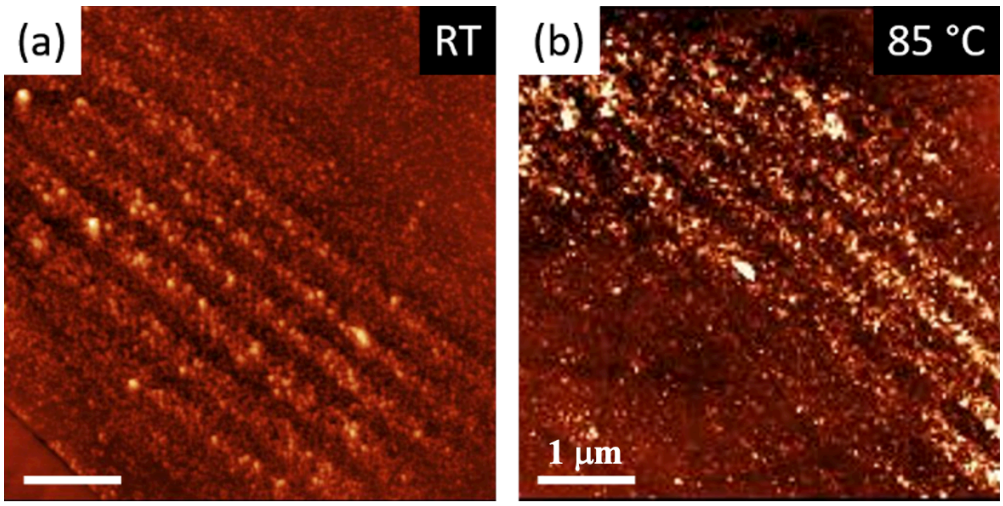

Figure 4. AFM topography after photodeposition of MnO_x at (a) Room temperature (RT) and (b) at 85 °C. Dark-to-light vertical scales: (a) 32 nm (b) 14 nm.

When interpreting the images in Fig. 4, it is important to recognize there are vertical height differences on the surface caused by the domain structure, because the images are recorded at room temperature where the sample is monoclinic. Therefore, it is necessary to quantify the height differences caused by the ferroelastic domain structure and by the reaction product. This is illustrated in Fig. 5, where the heights of the domains are measured (at room temperature) before and after the photoanodic deposition of PbO_x at 85 °C. Figure 5(a) shows a topographic AFM image of the clean surface. The surface profile of three pairs

of domains (averaged over 128 pixels along the domain direction) is taken from the area indicated by the black lines. This profile is shown as the solid line in Fig. 5(c). The height differences between the higher and lower domains (from left to right) are approximately 1.5 nm, 3.5 nm, and 4 nm. Figure 5(b) shows a topographic AFM image of the surface after the photoanodic deposition of PbO_x at 85 °C. The surface profile measured across the same three domains evaluated in Fig. 5(a), and also averaged over 128 pixels, is shown by the dashed line in Fig. 5(c). The height differences between the peaks and valleys for the same three domains are approximately 7.2 nm, 7.5 nm, and 12.5 nm. These are significantly greater for each domain when compared to the differences on the clean surface (1.5 nm, 3.5 nm, and 4 nm) and this is because more oxidized lead was deposited at the positions of the peaks than the valleys. This supports the assertion that surface charges remain on the sample at 85 °C, at the positions of the domains, even though the material is tetragonal.

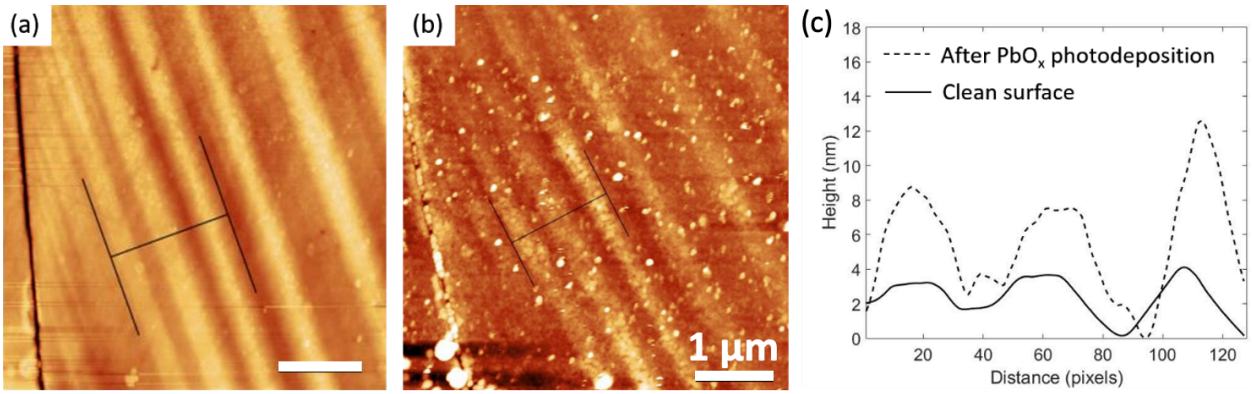

Figure 5. AFM topography of a grain (a) before and (b) after photodeposition of PbO_x at 85 °C . The topography profiles of the same three domains in both are shown in (c). The profiles are averaged over 128 pixels.

Past research has shown that while some domains are photoanodic, the others are photocathodic. [9] In other words, the reactivity of the alternating domains is complementary for the overall reaction. To demonstrate this here, the same sample used for photoanodic

reactions described above was used to promote the photocathodic reaction at room temperature. Note that attempts to conduct the photocathodic reaction at 85 °C were not successful because the reaction rate was so great and the morphology of the silver deposits so large that it was not possible to evaluate any spatial selectivity that might (or might not) be present. The SEM image in Fig. 6(a), taken after photocathodic deposition of silver, illustrates that small silver particles deposit on certain domains and form the characteristic ferroelastic striped pattern. To demonstrate complementarity of the reaction at 85 °C, an AFM image is shown in Fig. 6(b), of the same grain as in Fig. 6(a), taken after the photoanodic deposition of MnO_x at 85 °C; as expected, the topography of the deposits exhibit the familiar striped pattern of deposits. Close inspection of the widths of the domains (indicated by the arrows in the image) reveals that the MnO_x deposited on areas of the surface where Ag did not deposit, and vice versa. These results indicate that the surface charges of the high-temperature non-ferroelastic domains have the same sign (and complementarity) as the low temperature ferroelastic domains, suggesting that the origin of the surface charges is not arising from the ferroelastic domains alone.

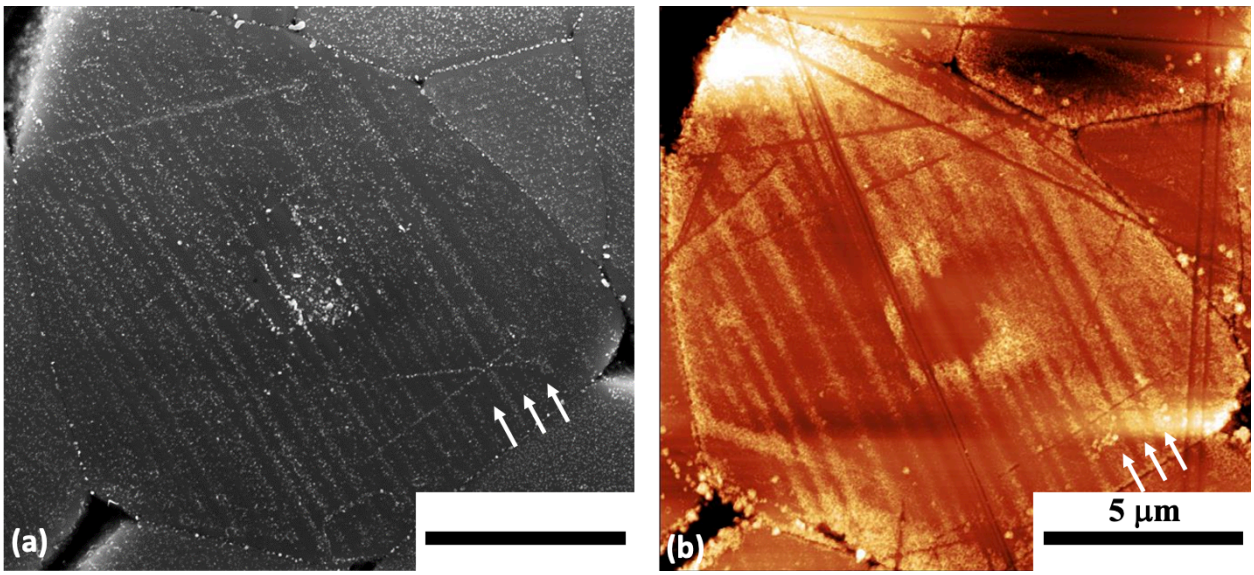

Figure 6. (a) SEM image of the surface after the photoreduction of Ag at room temperature. (b) Topographic AFM image after the photoanodic oxidation of Mn^{2+} at 85 °C

The observation that charged domains persist at 85 °C after the material has transformed to the tetragonal structure suggests that there are inhomogeneous distributions of charge point defects. This distribution is thought to arise from strain relief within the ferroelastic domains. When a sample is heated to 85 °C, for which the charge distribution was not obviously affected, was then cooled back below the transition temperature, the ferroelastic domain pattern is nearly the same as before heating through the transition. The structure is presumably preserved because the inhomogeneous distribution of point defects acts as a template to recreate the original domain structure. If the surface charge is related to point defects, then these defects should homogenize when the sample is annealed at a sufficiently high temperature for a sufficiently long time. To test this hypothesis, we imaged the domains before any treatment, after a 10 min anneal at 85 °C (tetragonal state), and then after a 10 h anneal at 400 °C (also tetragonal state). Piezoforce microscopy images of the same region of

a crystal are compared in Fig. 7. After the 10 min/85°C anneal, the domains are nearly unchanged, as in Figs. 4 through 6. However, after the 20h/ 400 °C anneal, conditions that are expected to promote homogenization of the defect distribution, the domain structure that forms on cooling differed substantially from before the treatment, with the widths of the domains and the boundaries between different variant clusters being altered. This same phenomenon was found in all areas imaged.

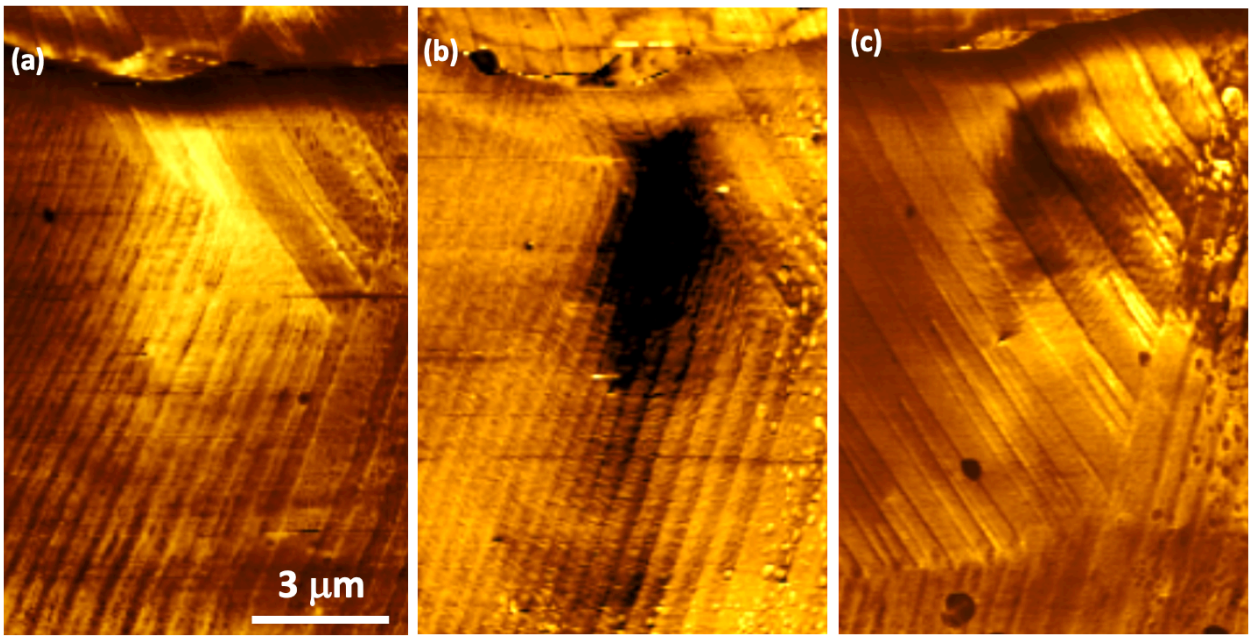

Figure 7. Out of plane amplitude contrast piezoforce microscopy images. (a) Before treatment. (b) After 10 min at 85 °C. (c) After 20 h at 400 °C.

Finally, we also examined the photochemical reactivity of single crystals, as a way of determining if the stresses imposed by neighboring crystals in the ceramic had an important influence on the domain selectivity. The diffraction pattern from the hydrothermally produced crystals (see Fig. S2) is consistent with expectation for $BiVO_4$. In addition to having free boundaries without stresses from neighboring crystals, the hydrothermally grown

crystals were synthesized at 200 °C, which is below the $BiVO_4$ ferroelastic transition temperature. Therefore, these crystals have not transformed from the higher temperature tetragonal structure, so it is interesting to compare their photochemical reactivity to that of the stressed crystals in ceramics that have been studied in the past. A backscattered electron contrast image of a hydrothermally grown crystal is shown in Figure 8a and the contrast associated with the ferroelastic domains is clearly observable. A secondary electron contrast image of the same crystal after the photoreduction of silver is show in Figure 8b. It is clear that the silver accumulates on the darker of the two domains visible in Figure 8a. The spatially selective reduction of silver on a subset of domains is consistent with observations from ceramic polycrystals, so we conclude that the internal stresses within the polycrystal do not create the charged domains that reduce Ag^+ from solution.

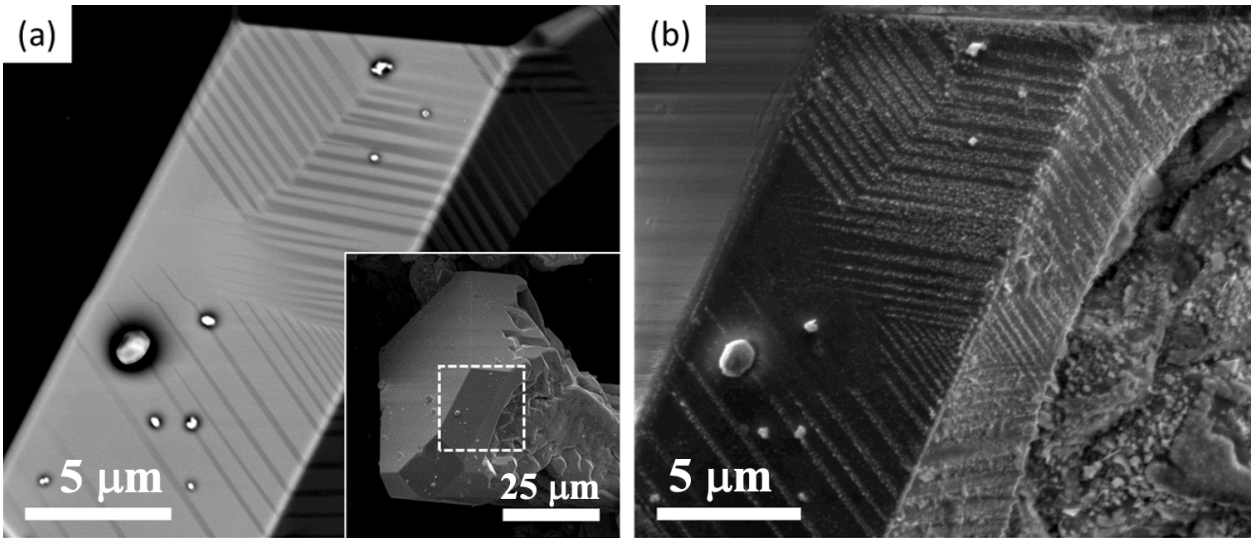

Figure 8. (a) BSE image of two facets of a hydrothermally-grown $BiVO_4$ crystal. The entire crystal is shown in the inset. The BSE image is of the area inside the dashed line. (b) SE image of the same two facets after photodeposition of Ag^+.

4. Discussion

The results presented here demonstrate that the photoanodic deposition reaction occurs preferentially in a striped pattern reminiscent of the preexisting monoclinic, ferroelastic domain structure even after the sample has transformed to the tetragonal, non-ferroelastic structure. Because the spatial distribution of the reaction products mimics the preexisting domain structure, it seems clear that the prior existence of the domains is necessary. This is consistent with prior studies by Munprom et al.[9], who demonstrated that there was no spatial selectivity at room temperature for tetragonal samples that were co-doped at x=0.175 (as compared to x=0.08 for our samples). At the x=0.175 composition, the samples were not in the monoclinic phase at any time during processing[22] and, therefore, ferroelastic domains were also never present. In the current case of x=0.08, ferroelastic domains existed at room temperature throughout the duration of the work and were eliminated only during the photoanodic reactions at 85 °C (and longer anneals at 400 °C). In other words, the room temperature domain structure must create the charge distribution that is still observed after they disappear at 85 °C. This might plausibly happen by several mechanisms, discussed below.

One possible explanation for the charged domains is the segregation of charged point defects to differently stressed ferroelastic domains. This is analogous to how point defects migrate in response to stresses during creep. For example, assume oxygen vacancies are uniformly distributed in the tetragonal phase and have a free energy of formation ε_V and a volume Ω. After the transformation to the monoclinic structure, ferroelastic domains are formed and alternating domains will be subject to tensile and compressive stresses ($\pm\sigma$). As a result, the free energy of formation of vacancies in the two domains will be $\varepsilon_V \pm \sigma\Omega$, where

the sign depends on the applied stress in the domain. As a result, there will be a different equilibrium concentration of vacancies in adjacent domains and a gradient in the chemical potential that will cause vacancies to diffuse down the gradient to accumulate in the domain with smaller formation energy and deplete from the domain with the greater formation energy. In the supplemental materials (see Estimate of the defect flux), an equation is derived for the flux of vacancies from domains of higher vacancy formation energy to lower vacancy formation energy; the result indicates that the vacancy flux increases as the diffusion coefficient of vacancies increases, the stress increases, and the domain size decreases. As long as the vacancies are charged, this will create alternating domains with opposite relative charges and, according to calculations reported by Yin et al.[24], oxygen vacancies are shallow donors and should be partially ionized. It should be emphasized that while the argument above was made for oxygen vacancies, it would apply to any mobile, charged defect that alters the crystal volume.

It has been reported that oxygen vacancies are the dominant intrinsic defect in $BiVO_4$.[25] It has also been reported that the region within about 5 nm of the surface is enriched in oxygen vacancies to a concentration as great as 15 %.[26] While oxygen vacancy diffusion in most compounds with the scheelite structure is difficult, $BiVO_4$ is an exception.[27] Extrapolating oxygen diffusion coefficients reported by Yang et al.[27] to the transition temperature (~ 530 K), the diffusion coefficient is estimated to be 1×10^{-11} cm^2/s. In this case, it would take 10 s at 530 K for oxygen to diffuse 250 nm, which is the observed length scale of the domains. With this diffusion rate, the oxygen ions have the mobility needed to redistribute during cooling after the phase transformation to partially relieve the compressive and tensile stresses in alternating domains. A similar stress driven differential

segregation of mobile $CH_3NH_3^+$ ions to different domains in $CH_3NH_3PbI_3$ films has been reported by Liu et al.[28].

It should be noted that in the present experiment, the sample transformed to the non-ferroelastic tetragonal structure at the reaction temperature (85 °C). The sample was at this temperature for only about five min (a limitation of the experiment imposed by the accelerated evaporation of the liquid at this temperature). Once again, extrapolating from the data presented by Yang et al.[27], the oxygen diffusion coefficient is estimated to be 5×10^{-14} cm^2/s, so the root mean square displacement in five min is 90 nm, smaller than the typical size of a domain. Therefore, it is plausible that the vacancy distributions are stable over the length scale of the experiment. The existence of a residual domain-related inhomogeneous vacancy distribution would explain the observation that the pattern of domains after heating and cooling is almost exactly the same (see Fig. 2). Assuming that the initial ferroelastic domain structure led to a quasi-equilibrium point defect distribution to relieve stresses associated with the domain structure, and that the distribution was mostly maintained during the 5 min, 85 °C photodeposition experiment, then it seems plausible that the defect distribution would stimulate the nucleation and growth of a new but similar ferroelastic domain structure after cooling.

Other charged defects that might be play a role in this process are substitutional Na and Mo. The Na (Mo) atoms on Bi (V) sites are very shallow acceptors (donors) [24] and when ionized would create a distribution of charge, similar to what was discussed above for oxygen vacancies. Furthermore, it has been reported that surface Mo can lead to increased charge transfer efficiency, increasing the reaction rate.[29] Finally, because the concentrations of Na and Mo influence the ferroelastic transition temperature, large excursions in

composition might lead to local volumes that transform more easily than expected or that resist transformation. If this were to lead to tetragonal and monoclinic domains, this might create boundaries between phases with different band gaps[30] that could influence reactivity[31,32], although we have no evidence for this. Therefore, there are several possible mechanisms by which inhomogenous Na and Mo distributions might lead to the observed spatially selective reactivity. However, it should be noted that charged ferroelastic domains are observed in undoped $BiVO_4$, indicating that Na and Mo are not necessary to create charged domains. While the temperature of the phase transformation in undoped $BiVO_4$ (255° C) eliminates the possibility of aqueous photochemical experiments, in the future hot-stage Kelvin probe force microscopy might provide useful information about the surface charge on the undoped material above and below the transition temperature.

It is also possible that the surface charges that remain after the transformation to the tetragonal structure are related to surface adsorption. For example, it has been reported that surface charge on domains at the $BaTiO_3$ surface could still be measured for several minutes at temperatures above the ferroelectric transition temperature.[33] The residual charges are thought to be caused by adsorbed polar molecules on the surface that remain immediately after the transition, but slowly dissipate. It is likely that this type of adsorption occurs in our experiment. However, it also seems likely that the deposition of reaction products would displace such adsorbates and disrupt this charge. Therefore, the segregation of charged defects is thought to be the more plausible explanation for the spatially selective photoanodic deposition of reaction products and the templating of the domain structure on cooling.

5. Conclusions

The observation of spatially selective reactivity above the ferroelectric transition temperature indicates that flexoelectric phenomena associated with internal stresses do not cause the domain charges. The results are consistent with the segregation of charged point defects, which accumulate in specific domains to relieve internal stresses but also create a locally heterogeneous distribution of charge correlated to the domain structure. The inhomogeneous distribution is maintained for brief anneals above the critical temperature, but longer higher temperature anneals erase the distribution and lead to the formation of a new domain structure.

Acknowledgements

The authors acknowledge the support of National Science Foundation through grants DMR 1609369 and DMR 2016267, and use of the Materials Characterization Facility at Carnegie Mellon University supported by grant MCF-677785.

References Cited

[1]Moniz, S. J. A., Shevlin, S. A., Martin, D. J., Guo, Z.-X., and Tang, J., Visible-light driven heterojunction photocatalysts for water splitting - a critical review, Energy Environ Sci. 2015;8(3):731-59.

[2]Park, Y., McDonald, K. J., and Choi, K.-S., Progress in bismuth vanadate photoanodes for use in solar water oxidation, Chem Soc Rev. 2013;42(6):2321-37.

[3]Trzesniewski, B. J., and Smith, W. A., Photocharged $BiVO_4$ photoanodes for improved solar water splitting, J Mater Chem A. 2016;4(8):2919-26.

[4]Zachaus, C., Abdi, F. F., Peter, L. M., and van de Krol, R., Photocurrent of $BiVO_4$ is limited by surface recombination, not surface catalysis, Chem Sci. 2017;8(5):3712-19.

[5]Li, R., Han, H., Zhang, F., Wang, D., and Li, C., Highly efficient photocatalysts constructed by rational assembly of dual-cocatalysts separately on different facets of $BiVO_4$, Energy Environ Sci. 2014;7(4):1369-76.

[6]Li, R., Zhang, F., Wang, D., Yang, J., Li, M., Zhu, J., Zhou, X., Han, H., and Li, C., Spatial separation of photogenerated electrons and holes among {010} and {110} crystal facets of $BiVO_4$, Nat. Commun. 2013;4(1432.

[7]Munprom, R., Salvador, P. A., and Rohrer, G. S., The orientation dependence of the photochemical reactivity of $BiVO_4$, J. Mater. Chem. A. 2015;3(5):2370-77.

[8]Munprom, R., Salvador, P. A., and Rohrer, G. S., Polar Domains at the Surface of Centrosymmetric $BiVO_4$, Chem. Mater. 2014;26(9):2774-76.

[9]Munprom, R., Salvador, P. A., and Rohrer, G. S., Ferroelastic domains improve photochemical reactivity: a comparative study of monoclinic and tetragonal $(Bi_{1-0.5x}Na_{0.5x})(V_{1-x}Mo_x)O_4$ ceramics, J. Mater. Chem. A. 2016;4(8):2951-59.

[10]Bierlein, J. D., and Sleight, A. W., Ferroelasticity in $BiVO_4$, Solid State Comm. 1975;16(1):69-70.

[11]Sleight, A. W., Chen, H. Y., Ferretti, A., and Cox, D. E., Crystal-growth and structure of $BiVO_4$, Mater Res Bull. 1979;14(12):1571-81.

[12]Manolikas, C., and Amelinckx, S., Ferroelastic domains in $BiVO_4$, Phys Stat Sol A. 1980;60(1):167-72.

[13]Nepochatenko, V. A., and Dudnik, E. F., Ferroelastic domain walls in BiVO4, Crystallography Reports. 2005;50(1):102-07.

[14]Pisat, A. S., Rohrer, G. S., and Salvador, P. A., Spatial selectivity of photodeposition reactions on polar surfaces of centrosymmetric ferroelastic gamma-WO_3, J Mater Chem A. 2017;5(18):8261-66.

[15]Zitello, K. E., Salvador, P. A., and Rohrer, G. S., Influence of surface orientation on the photochemical reactivity of $CaTiO_3$, J Am Ceram Soc. 2020;103(8):4498-506.

[16]Salje, E., and Viswanathan, K., Physical-properties and phase-transitions in WO_3, Acta Cryst A. 1975;A 31(MAY1):356-59.

[17]Yashima, M., and Ali, R., Structural phase transition and octahedral tilting in the calcium titanate perovskite $CaTiO_3$, Solid State Ionics. 2009;180(2-3):120-26.

[18]Kim, Y., Morozovska, A. N., Kumar, A., Jesse, S., Eliseev, E. A., Alibart, F., Strukov, D., and Kalinin, S. V., Ionically-Mediated Electromechanical Hysteresis in Transition Metal Oxides, Acs Nano. 2012;6(8):7026-33.

[19]Li, Q., Lu, T., Schiemer, J., Laanait, N., Balke, N., Zhang, Z., Ren, Y., Carpenter, M. A., Wen, H. D., Li, J. Y., Kalinin, S. V., and Liu, Y., Giant thermally-enhanced electrostriction and polar surface phase in $La_2Mo_2O_9$ oxygen ion conductors, Phys Rev Mater. 2018;2(4):
[20]Yudin, P. V., and Tagantsev, A. K., Fundamentals of flexoelectricity in solids, Nanotechnology. 2013;24(43):
[21]Necas, D., and Klapetek, P., Gwyddion: an open-source software for SPM data analysis, Cent Eur J Phys. 2012;10(1):181-88.
[22]Zhou, D., Pang, L.-X., Wang, H., Guo, J., Yao, X., and Randall, C. A., Phase transition, Raman spectra, infrared spectra, band gap and microwave dielectric properties of low temperature firing $(Na_{0.5x}Bi_{1-0.5x})(Mo_xV_{1-x})O_4$ solid solution ceramics with scheelite structures, J Mater Chem. 2011;21(45):18412-20.
[23]"Crystalmaker: Software for Visulaizing Crystals and Molecules."
[24]Yin, W. J., Wei, S. H., Al-Jassim, M. M., Turner, J., and Yan, Y. F., Doping properties of monoclinic $BiVO_4$ studied by first-principles density-functional theory, Phys Rev B. 2011;83(15):
[25]Abdi, F. F., Savenije, T. J., May, M. M., Dam, B., and van de Krol, R., The Origin of Slow Carrier Transport in $BiVO_4$ Thin Film Photoanodes: A Time-Resolved Microwave Conductivity Study, J Phys Chem Lett. 2013;4(16):2752-57.
[26]Rossell, M. D., Agrawal, P., Borgschulte, A., Hebert, C., Passerone, D., and Erni, R., Direct Evidence of Surface Reduction in Monoclinic $BiVO_4$, Chem Mater. 2015;27(10):3593-600.
[27]Yang, X. Y., Fernandez-Carrion, A. J., Wang, J. H., Porcher, F., Fayon, F., Allix, M., and Kuang, X. J., Cooperative mechanisms of oxygen vacancy stabilization and migration in the isolated tetrahedral anion Scheelite structure, Nat Commun. 2018;9(
[28]Liu, Y. T., Collins, L., Proksch, R., Kim, S., Watson, B. R., Doughty, B., Calhoun, T. R., Ahmadi, M., Ievlev, A. V., Jesse, S., Retterer, S. T., Belianinov, A., Xiao, K., Huang, J. S., Sumpter, B. G., Kalinin, S. V., Hu, B., and Ovchinnikova, O. S., Chemical nature of ferroelastic twin domains in $CH_3NH_3PbI_3$ perovskite, Nat Mater. 2018;17(11):1013-+.
[29]Kim, D., Zhang, Z., and Yong, K., Synergistic doping effects of a ZnO:N/$BiVO_4$:Mo bunched nanorod array photoanode for enhancing charge transfer and carrier density in photoelectrochemical systems, Nanoscale. 2018;10(43):20256-65.
[30]Jo, W. J., Kang, H. J., Kong, K. J., Lee, Y. S., Park, H., Lee, Y., Buonassisi, T., Gleason, K. K., and Lee, J. S., Phase transition-induced band edge engineering of $BiVO_4$ to split pure water under visible light, PNAS. 2015;112(45):13774-78.
[31]Bickley, R. I., Gonzalezcarreno, T., Lees, J. S., Palmisano, L., and Tilley, R. J. D., A structural investigation of titanium-dioxide photocatalysts, J Solid State Chem. 1991;92(1):178-90.
[32]Wang, X., Xu, Q., Li, M., Shen, S., Wang, X., Wang, Y., Feng, Z., Shi, J., Han, H., and Li, C., Photocatalytic Overall Water Splitting Promoted by an alpha-beta phase Junction on Ga_2O_3, Angew Chem Int Ed Engl. 2012;51(52):13089-92.
[33]Kalinin, S. V., and Bonnell, D. A., Local potential and polarization screening on ferroelectric surfaces, Physical Review B. 2001;63(12):125411.

Supplemental Information for: The origin of charged domains on the surface of ferroelastic $BiVO_4$ co-doped with Na and Mo.

Ajay S. Pisat, Jackson C. Adler, Paul A. Salvador, Gregory S. Rohrer

Department of Materials Science and Engineering, Carnegie Mellon University, Pittsburgh, Pennsylvania 15213, USA

The diffraction pattern of the $(Bi_{1-0.5x}Na_{0.5x})(V_{1-x}Mo_x)O_4$, x = 0.08 ceramic is illustrated in Fig. S1. The diffraction pattern of hydrothermally grown $BiVO_4$ crystals is illustrated in Fig. S2. The patterns conform to the expected pattern for monoclinic $(Bi_{1-0.5x}Na_{0.5x})(V_{1-x}Mo_x)O_4$ and $BiVO_4$.

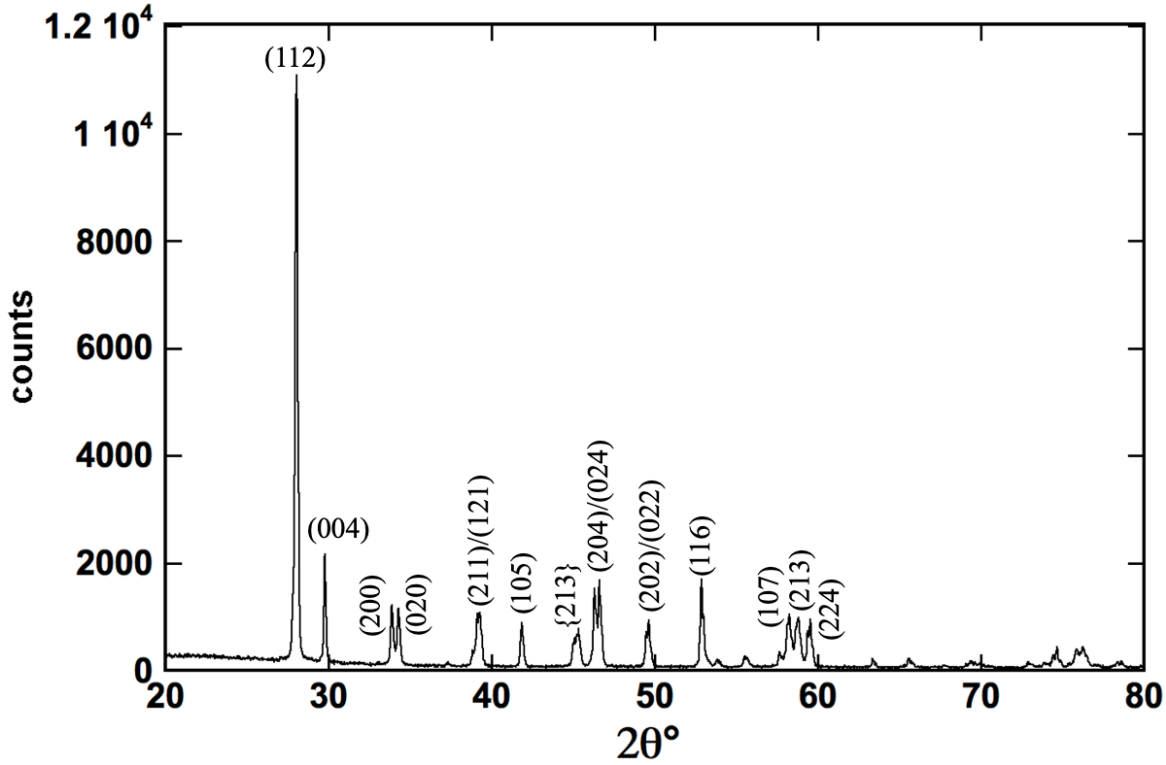

Figure S1. X-ray diffraction pattern of the Na, Mo co-doped sample, $(Bi_{1-0.5x}Na_{0.5x})(V_{1-x}Mo_x)O_4$, x = 0.08.

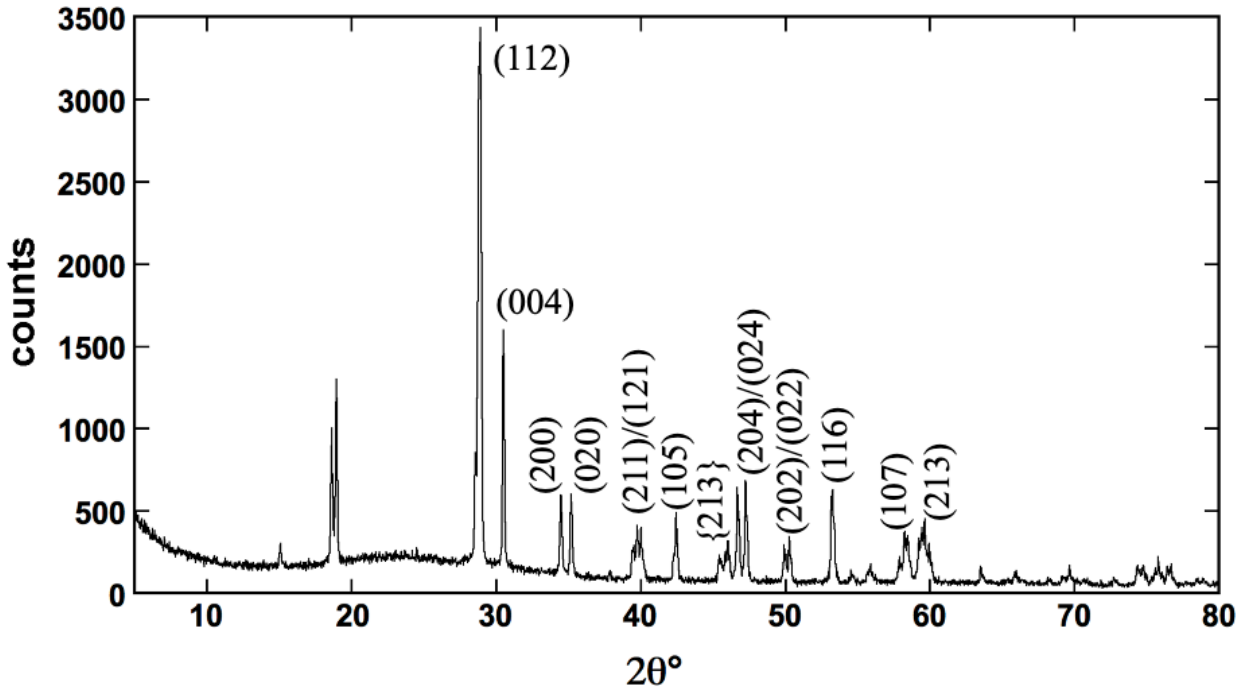

Figure S2: X-ray diffraction pattern of hydrothermally grown $BiVO_4$ crystals.

Estimate of the defect flux

To estimate the flux of vacancies between domains, we begin by assuming that in the unstressed crystal before the transformation, the vacancy concentration is:

$$n_V = exp\left(-\frac{\varepsilon_V}{kT}\right)$$

In domains subjected to tensile stress, it is easier to form vacancies (creating excess volume), so the vacancy formation energy (ε_V^{ten}) will be reduced by the factor of $\sigma\Omega$.

$$\varepsilon_V^{ten} = \varepsilon_V - \sigma\Omega$$

In the domains subjected to compression, it will be more difficult to create the excess volume needed to accommodate a vacancy, so the vacancy formation energy (ε_V^{comp}) will be increased by the factor of $\sigma\Omega$.

$$\varepsilon_V^{comp} = \varepsilon_V + \sigma\Omega$$

The equilibrium concentrations in the tensile and compressive domains are, therefore:

$$n_V^{ten} = exp\left(\frac{-(\varepsilon_V - \sigma\Omega)}{kT}\right) = n_V\, exp\left(\frac{\sigma\Omega}{kT}\right)$$

$$n_V^{comp} = exp\left(\frac{-(\varepsilon_V + \sigma\Omega)}{kT}\right) = n_V\, exp\left(-\frac{\sigma\Omega}{kT}\right)$$

The gradient from the compressive domain to the to the tensile domain is:

$$\Delta n_V = n_V\left[exp\left(-\frac{\sigma\Omega}{kT}\right) - exp\left(\frac{\sigma\Omega}{kT}\right)\right]$$

Fick's first law can be used to determine the flux that would result from this gradient. Assuming the domain width, r, is the dimension over which the gradient is established, the vacancy flux (J_V) is:

$$J_V = -D_V\frac{\Delta n_V}{\Delta x} = -D_V\frac{n_V}{r}\left[exp\left(-\frac{\sigma\Omega}{kT}\right) - exp\left(\frac{\sigma\Omega}{kT}\right)\right]$$

Where D_V is the vacancy diffusion coefficient. Because $\sigma\Omega \ll$ kT, we can use a Taylor expansion to approximate $\exp(x) - \exp(-x) \approx 2x$ and the flux is:

$$J_V = \frac{2D_V n_V \Omega\sigma}{rkT}$$

So, the flux of vacancies from compressive to tensile domains would increase as the diffusion coefficient of vacancies increases, the stress increases, and domain size decreases.

References Cited

[1] Y. Kim, M. Alexe, E.K.H. Salje. Nanoscale properties of thin twin walls and surface layers in piezoelectric WO3-x, Applied Physics Letters 96 (2010), http://dx.doi.org/10.1063/1.3292587.